https://doi.org/10.22226/2410-3535-2022-4-269-275

Structure formation and physical-mechanical properties of Al-Mg alloy with microadditions of graphene

I. G. Brodova[†,1], L. A. Yolshina[2], D. Yu. Rasposienko[1], R. V. Muradymov[2], I. G. Shirinkina[1], S. V. Razorenov[3], A. N. Petrova[1], E. V. Shorokhov[4]

[†] brodova@imp.uran.ru

[1]Mikheev Institute of Metal Physics, UB of the RAS, Ekaterinburg, 620108, Russia
[2]Institute of High-Temperature Electrochemistry, UB of the RAS, Ekaterinburg, 620990, Russia
[3]Institute of Problems of Chemical Physics, RAS, Chernogolovka, 142432, Russia
[4]Federal State Unitary Enterprise "Russian Federal Nuclear Center — Zababakhin All-Russia Research Institute of Technical Physics", Snezhinsk, 456770, Russia

Composites based on Al-Mg alloy, reinforced with graphene nanofilms, were obtained by in situ synthesis under a layer of salt melt. Using SEM and HRTEM, the morphological and dimensional characteristics of the structural components of composites with different contents of graphene were studied. An experiment on dynamic compression of composites by the Kolsky method was carried out, dynamic properties were measured, and the evolution of a cast structure during high-speed deformation was considered. For the first time, the dynamic properties of composites under loading by plane shock waves have been determined. The dynamic properties of aluminum matrix composites are compared depending on the properties of the non-reinforced alloy.

Keywords: aluminum, composite, graphene, structure, dynamic properties, transmission electron microscopy, high resolution, hardness.

1. Introduction

In recent years, the development of efficient methods for the production of metal matrix composites has become a crucial task of the material physics [1–5]. AlMg alloys are well-known materials widely used for various industrial applications requiring a good combination of corrosion resistance, ductility, viscosity, and weldability [6]. The mechanical strength of AlMg alloys depends on the content of magnesium since it is an effective solid solution reinforcing additive. The ultimate tensile strength of annealed alloys containing more than 6% Mg (here and below, the concentrations of elements are given in wt.%) is UTS = 300 MPa. A decrease in the content of Mg results in a decrease in the mechanical strength of Al-Mg alloys. Therefore, the reinforcement of such materials is of current research interest and can be addressed by designing composites based on AlMg matrix, such as, for example, the composite based on AMg5 alloy reinforced with TiB_2 nanoparticles [2,3]. There is also intensive research into the characteristics of aluminum matrix composites with various carbon-containing additives, such as nanotubes, fullerenes, graphene [7–11].

Graphene occupies a unique position among carbon-based nanomaterials. Several times, it has been demonstrated that its introduction into an aluminum matrix improves the properties [4,9,12]. According to [13–16], *in-situ* synthesis in a molten metal matrix layer under molten salts is an efficient technique for producing graphene- and diamond-reinforced aluminum matrix composites. Thus, the produced aluminum matrix composites containing 0.10–0.13% graphene exhibit enhanced mechanical properties both in the as-cast [17] and in the deformed state [18].

The present work aims to study the structure formation, and deformation behaviour of AlMg alloy-based graphene-reinforced composites synthesized *in-situ*.

2. Materials and methods

The object of the study was composites based on an Al-1.8% Mg alloy (type AA 5154) reinforced with a graphene micro additive in an amount of 0.22%. The synthesis of such aluminum matrix composites, described in detail in [13–16], involved the interaction of a molten AlMg alloy with a carbon-containing precursor in a molten alkali halide medium (sodium, potassium chlorides with an addition of ammonium fluorides). The ascorbic acid powder was used as a carbon-containing additive in synthesizing composites based on AlMg alloys. The synthesis temperature was 700–750°C, the time of holding the liquid Al-Mg alloy in the molten salt containing 0.1–2.0% ascorbic acid $C_6H_8O_6$ was 1–3 h. The synthesis of the carbon atoms was a one-step process taking place directly in the molten alloy. Initially, in the process of self-assembly, carbon clusters are formed, followed by the appearance of continuous nanofilms that are evenly distributed in the volume of the solidifying melt.

The structure and properties of the composites were compared with the corresponding characteristics of the

industrial alloy Al_3Mg. Samples in the form of cylinders with a diameter of 14 mm and a height of 100 mm were cast into a copper mold.

Spectroscopic analysis was undertaken to study the content of carbon and the basic components of the synthesized composites. The results are listed in Table 1.

Certification of carbon inclusions in the Al-Mg matrix was carried out by energy dispersive analysis on a scanning electron microscope (Quanta-200) and by Raman spectroscopy using a Renishaw U 1000 micro-Raman spectrometer (UK) connected to a Leica DML microscope equipped with 50× and 100× magnification lenses. The spectra were processed and analyzed using the built-in Wire-30 software and the specialized software package Fityk 0.9.8. The elemental composition on the surface of the synthesized composites was determined from photoelectron spectra obtained using a KAlpha X-ray photoelectron spectrometer (UK).

The dynamic properties of the composites with a varying graphene content were analyzed in two ranges of strain rate during dynamic compression of the samples 8 mm in diameter and 4 mm in height in a split Hopkinson-Kolsky bar ($\dot{\varepsilon}=1.3\times10^3$ s^{-1}, the velocity of the striker is 6.6 m/s) [19] and during shock-wave loading ($\dot{\varepsilon}=3.5\times10^5$ s^{-1} the velocity of the aluminum plate impactor is 600 m/s) of a disk sample 2 mm thick [20]. In addition, Brinell hardness HB and the microhardness Hv of the synthesized composites were determined (PMT-3 device, Russia).

The macrostructure of the samples was examined using a NEOPHOT-32 optical microscope and a QUANTA 200, Tescan MIRA3 and Zeiss Sigma VP scanning electron microscopes, an Auriga CrossBeam Workstation (Carl Zeiss NTS, Germany), equipped with an Inca Energy 350X-MAX EDS spectrometer (Oxford Instruments, UK) scanning electron microscopes (SEM). The samples were prepared for structural analysis by mechanical polishing with a diamond suspension. The finishing polishing was performed using a suspension of colloidal silicon dioxide. The fine structure of the samples was studied on a Tecnai G 30 Twin transmission electron microscope (TEM) with 300 kV accelerating voltage. The samples for fine structure studies were prepared by jet polishing on TenuPol-5 device in the solution of 20% nitric acid and 80% methanol at the temperature of −25°C and the voltage of 15 – 20 V. The XRD analysis was performed on an Empyrean (PANalytical) diffractometer at ambient temperature with Cu-K_α radiation.

Table 1. Chemical composition of the synthesized alloys.

Denomination	Mg	C	Mn	Si
Al3Mg	3.0	-	0.3	0.4
AlMgGr	1.8	0.22	0.3	0.4

3. Results and discussion

3.1. Characterization of AlMgGr composites

The carbon inclusions in the matrix look like thin transparent nanofilms with linear dimensions approaching tens of μm (indicated by 1 – 3 in Fig. 1a). The purity and structural modification of the carbon phase in the volume of the Al-Mg matrix was studied by Raman spectroscopy [21, 22].

The Raman spectrum of the carbon inclusions given in Fig. 2 a contains a characteristic G peak at 1584 cm^{-1}, D peak at 1347 cm^{-1} and 2D peak at 2686.6 cm^{-1}, which is indicative of sp^2-hybridised carbon, i. e., graphene [21]. The analysis of the carbon peaks intensity ratio allows the determination of the structural properties of graphene [22]. The intensity ratio of 2D and G bands, I2D/IG, was found to be 0.74, which implies the formation of bilayer graphene. The defective nature of the graphene is indicated by the fact that the D and G peaks differ little in intensity, and the splitting of G peak and the presence of D peak of similar intensity are related to the appearance of five- and seven-fold rings in the graphene structure.

In addition to recording the spectra of graphene on a cross-section of an AlMgGr composite, some of its samples were dissolved in a 20% hydrochloric acid solution. Graphene flakes floating on the surface of the acid were caught on a substrate, photographed (Fig. 1b), and a Raman spectrum (Fig. 2 b) was also taken from them.

After dissolution in 20% HCl, it is evident that large transparent nanofilms of graphene with characteristic angles 120° with a very similar Raman spectrum a characteristic G peak at 1578 cm^{-1}, D peak at 1339 cm^{-1} and 2D peak at 2674 cm^{-1} were obtained. The difference of the values of the ratio of the bands intensiv I_{2D}/I_D, wich provides information on the ordering of graphene layer [23], are 0.74 (2 layers graphene) for graphene inside ingot and 1 (2 layers graphene) for free nanofilm of graphene that can be caused by substrate influence.

X-ray photoelectron spectroscopy indicates that the introduction of graphene into the AlMgGr composite

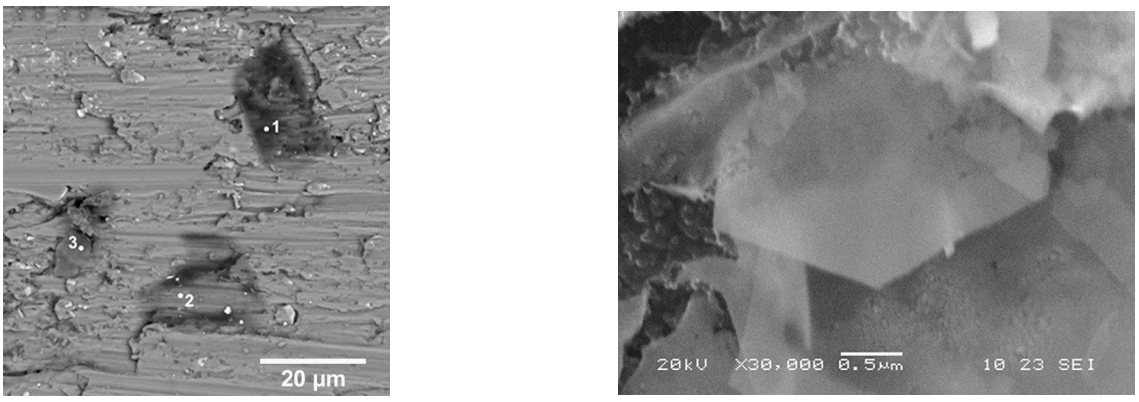

a b

Fig. 1. SEM images of the graphene nanofilm in the matrix of AlMgGr composite (a) and after it dissolution in 20% HCl (b).

causes significant changes in the electronic state of the cross-sectional surface of the sample. Figure 3 a contains the XPS spectrum of the composite, while Figures 3 b, 3 c, and d contain the high-resolution spectra for aluminium, magnesium, and carbon, respectively. The XPS spectrum of aluminum (Fig. 3 a) in the AlMgGr composite contains a peak characteristic of aluminum oxide at 75.03 eV, as well as two peaks of pure metallic aluminum at 72.8 and 73.14 eV. Deconvolution of the spectrum of carbon C1s (Fig. 3 d) gives asymmetric peaks with a dominant peak center at 284.9 eV, which confirms the sp^2-hybridization of carbon. In turn, the absence of a peak at 282 eV indicates that aluminum carbide is not formed during the synthesis of the composite.

3.2. Structure and properties of AlMgGr composites before and after dynamic compression

Metallographic studies indicate that the macrostructure of the ingots, the composition of which is given in Table 1, is practically identical, and the alternation of the structural zones is typical of mold casts. The external zone is 2 – 3 mm long and consists of columnar crystals, while the central zone is formed by equiaxed grains whose size does not depend on the chemical composition and is equal to 100 – 500 μm. The microstructure of AlMgGr composite consists of grains of Al solid solution with dendritic structure (Fig. 4 a) and fine-grained eutectic of skeletal morphology found at grain boundaries and dendritic cell boundaries (Fig. 4 b). The dendritic cell size in the mold casts of all the alloys is ≈5 μm.

EDS studies indicate that the eutectic is formed by different phases — Al_5Si_2 (Fe, Mn)$_3$ and Al_8Fe_2Si (light crystals of skeletal morphology, Fig. 4 b)) and the Mg_2Si phase (dark crystals, Fig. 4 b). The hardness of the composites depends both on the composition which is demonstrated in Table 2.

The comparison of the hardness of the AlMgGr composite and the Al3Mg alloy follows that doping with 0.22% graphene increases the hardness of the alloy only by 6%. A decrease

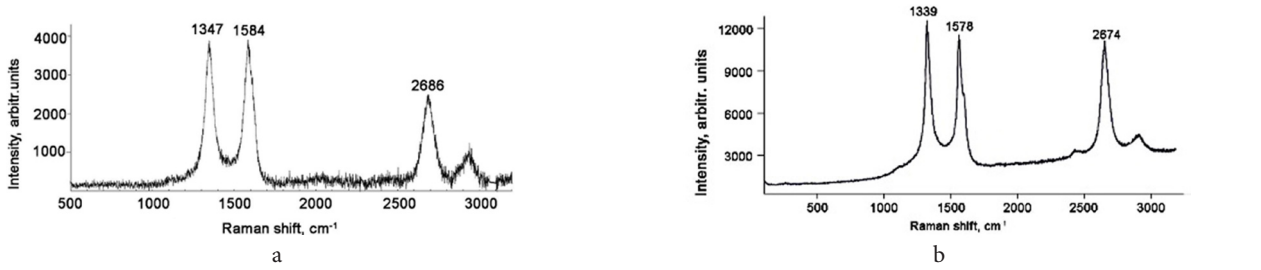

a b

Fig. 2. Raman spectrums of the graphene nanofilms in AlMgGr composite (a) and the graphene films obtained after dissolution of the composite in 20% HCl (b).

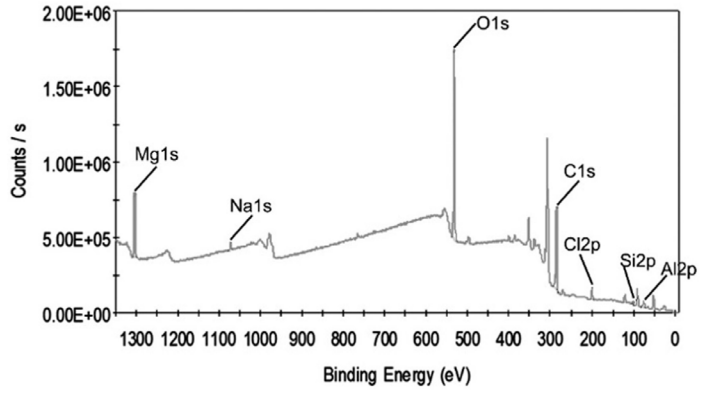

a

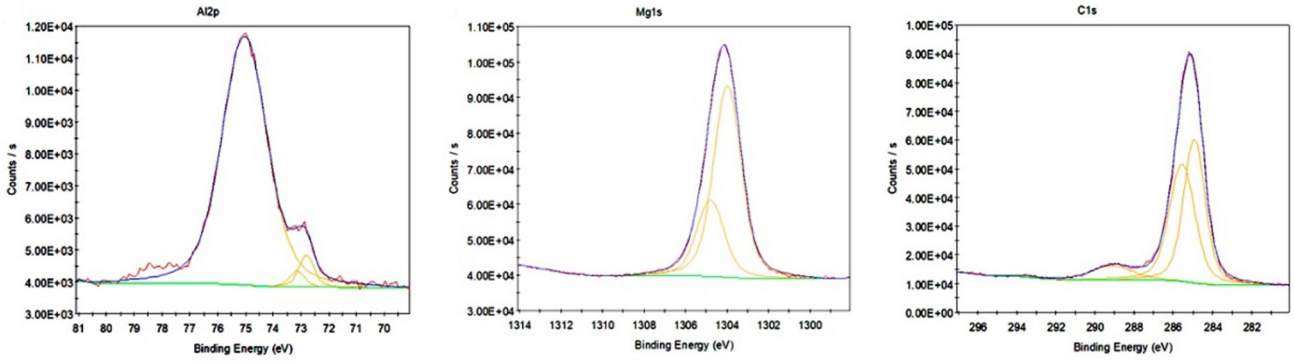

b c d

Fig. 3. (Color online) General photoelectron spectrum for AMgGr composite (a), high resolution photoelectron spectrums for Al (b), Mg (c) and C (d).

in the magnesium content in AlMgGr to 1.8% results in an expected reduction of hardness. An addition of 0.22% graphene does not compensate for the lack of magnesium in the matrix of the composites.

Figure 4c shows the macrostructure of the AMgGr composite after dynamic compression. The characteristic features of a structure deformed at a high rate include uneven refinement of matrix grains, which leads to a large spread in their sizes from hundreds to tens of microns (with an average size of ≈50 microns) and the formation of a modified eutectic localized clearly along grain boundaries.

The evolution of the composite microstructure under dynamic compression can be more thoroughly investigated by EBSD analysis. It is characterized by rather large grains (the average size is 40 – 50 μm) separated by high-angle boundaries — HABs (Fig. 5a,b). The grain-subgrain size change spectrum (Fig. 5c) demonstrates that the structural constituents vary significantly in size, ranging from 10 to 200 μm, with 65% of the grains-subgrains below 100 μm in size.

In the selected section of the structure, the amount of low-angle boundaries LGB is ≈90%, and the share of grain

Table 2. Hardness measurement results.

Composition	HB	Hv, MPa
Al3Mg	62	550
AlMgGr	58	580

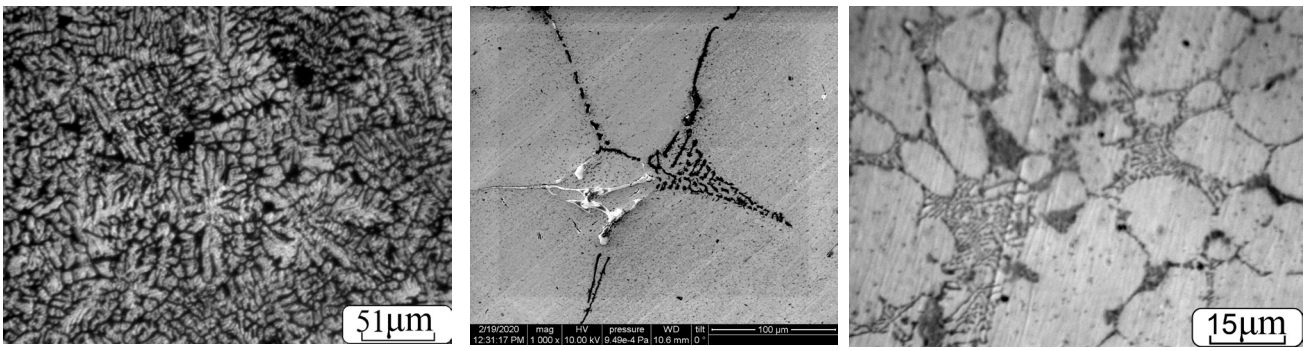

a b c

Fig. 4. AlMgGr composite microstructure before (a, b) and after dynamic compression (c).

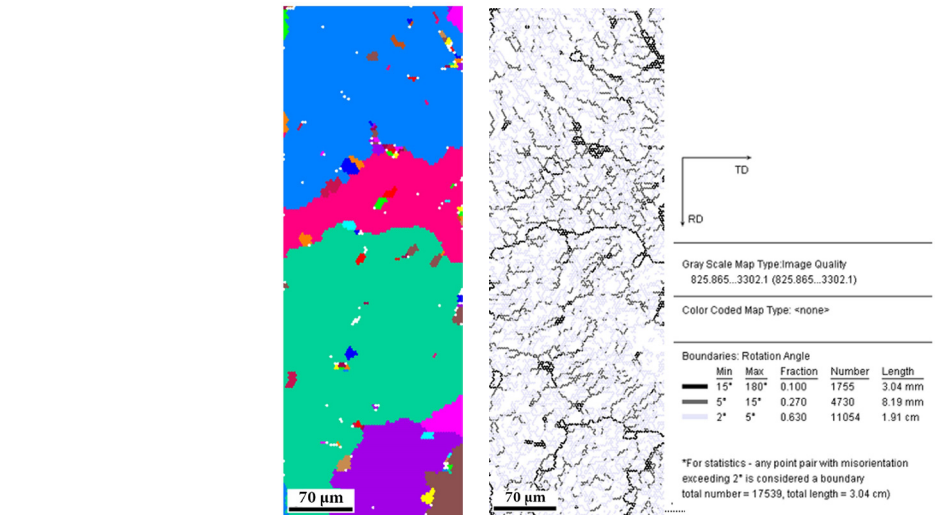

a b

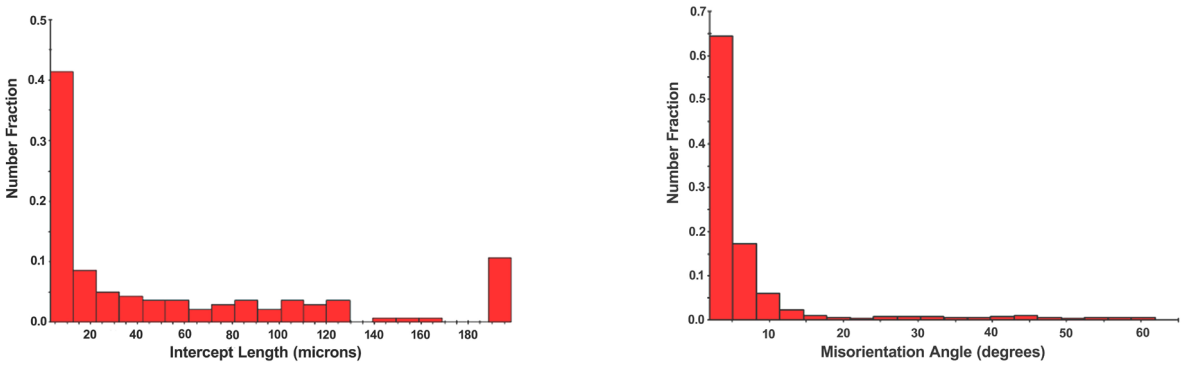

c d

Fig. 5. (Color online) EBSD maps of the composite after dynamic compression ($\dot{\varepsilon}=2\times10^3$ s^{-1}): orientation map (a), boundaries map (b), grain-subgrain size distribution (c), misorienation angle distribution (d).

boundaries with minimal misorientation accounts for 63% of all LGBs, and the average misorientation angle is 12° (Fig. 5 d). A well-developed network of LGBs inside the deformed grains indicates a high dislocation density. The formation of dislocation walls with a subsequent appearance of flat subgrain boundaries with medium-sized misorientation angles is related to the dynamic polygonization in the process of the composite deformation.

Figures 6 a, 6 b contain bright-field and dark-field images of the dispersed subgrain structure with a high dislocation density in the volume of the subgrains which confirms SEM data. The arrangement of graphene nanofilms in the Al matrix has been studied in detail in the investigations of AlGr composites and it has been proved using TEM data that they are bent and partially fragmented during deformation, located along the grain boundaries [17,18].

The AlMgGr composite exhibits an enhanced hardness after dynamic compression: under the described deformation conditions, the Hv of the matrix grew by 54% (Hv = 780 – 800 MPa).

The mechanical characteristics of the composites under quasi-static deformation with $\dot{\varepsilon}=1.3\times10^{3}$ s^{-1} and impactor velocity 6.6 m/s, determined from the dynamic stress-strain compression diagrams (Fig. 7), amounted to the conditional yield strength σ_T=125 MPa, conditional tensile strength σ_B = 277 MPa, against σ_T =111 MPa and σ_B = 270 MPa for non-reinforced Al3Mg alloy.

Analysis of the data presented above might lead one to the erroneous conclusion that the microaddition of graphene does not affect the properties. However, it should be taken into account that magnesium content in the composites is lower than in the Al3Mg reference alloy. According to GOST 4784-97 [24], an increase in the magnesium content from 2% to 3% increases the yield strength and tensile strength by 20 – 25 MPa, which indicates that the microaddition of graphene compensates for the lower amount of magnesium in the composite matrix. So the AlMgGr composite with the ratio of Mg : Gr = 1.80 : 0.22 and Al3Mg alloy have comparable properties.

The mechanical strength characteristics of the composites in the dynamic range of $\dot{\varepsilon}=3.5\times10^{5}$ s^{-1} were determined from the free surface velocity (wave) profiles (Fig. 8). The wave profiles for all the samples exhibit the behavior typical for spall fracture experiments [25, 26]. The specific features of the elastic-plastic transition depending on the composition of the samples become clear when we compare the shape and the amplitude of the elastic precursor. The lowest Hugoniot elastic limit and the highest spall strength are characteristic of Al3Mg alloy. The Hugoniot elastic limit of composites grows substantially, a sharp yield point appears, and the spall strength noticeably decreases. Table 3 contains the quantitative characteristics for the dynamic properties of the composites compared to AlMg alloy, where σ_{HEL} is the Hugoniot elastic limit, Y is the dynamic yield strength, σ_{SP} is

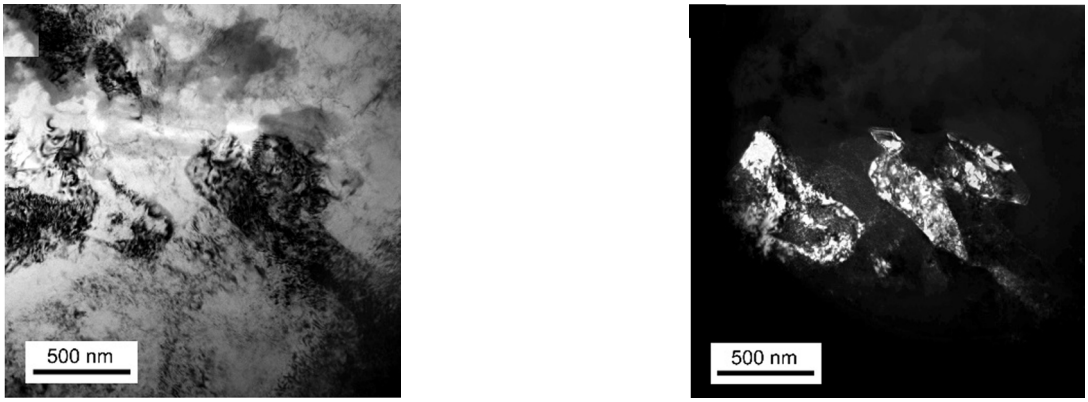

a b

Fig. 6. Grain structure images (TEM) of the AlMgGr composite after deformation using Hopkinson technique: bright field images (a); (200) Al dark field images (b).

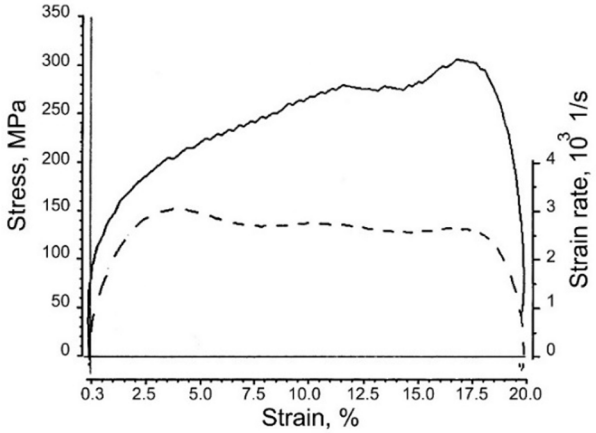

Fig. 7. Stress-strain diagram for the AlMgGr composite. The solid line corresponds to the stress-strain curve, and the dashed line corresponds to strain rate-strain curve.

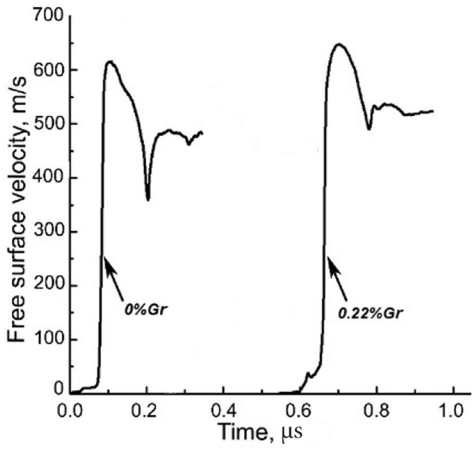

Fig. 8. Free surface velocity profiles for the Al3Mg alloy and the AlMgGr composite.

Table 3. Mechanical properties of the composites after dynamic compression.

Composition	P_{max}, GPa	σ_{HEL}, GPa	Y, GPa	σ_{SP}, GPa	Δh, mm
Al3Mg	4.7	0.08	0.04	2.08	0.31
AlMgGr	4.97	0.34	0.17	1.26	0.29

the spall strength, P is the maximum pressure of the impact compression, Δh is spall plate thickness.

The discovered 4-fold increase in the dynamic characteristics of the AlMgGr composite compared to the characteristics of the Al3Mg alloy confirms the enhancing effect of graphene nanoplatelets. Earlier investigations showed that graphene exhibits more pronounced enhancing properties if a submicrocrystalline matrix is formed in the aluminum-matrix composite [18]. Thus, the formation of SMC structure of the AlGr composite during intensive plastic deformation by dynamic compression was accompanied by the growth of the dynamic characteristics compared to the properties of SMC aluminum under similar conditions of deformation, i.e., in the case of a similar refinement of aluminum matrix structure, which can be explained by the fact that graphene nanoplatelets reside mainly at the grain-subgrain boundaries, forming barriers to the passing of dislocations and reducing the number of mobile defects. During the transition of the matrix from coarse grain to SMC state, the area of grain-subgrain boundaries increases sharply. Consequently, the carbon-containing component of the composite becomes a stronger barrier. It can be assumed that the exact mechanism of enhancement is characteristic of the AlMgGr composites.

Based on the theory of dynamic interaction between dislocations and structural defects, which considers different contributions from the forces of dynamic dislocation drag [27,28], taking into account the effect of the dislocation ensemble on the yield strength at high-speed deformation of the AlMgGr composites, the following should be considered. The value for the reinforcement of the AlMgGr composites will be made up of the sum of the force of dislocation drag by the graphene platelets, the force of the phonon friction and the force of dislocation drag by magnesium atoms. Due to a difference in size between the radii (R_{Mg}/R_{Al}=1.2), the role of this factor at $\dot{\varepsilon}=3.5\times10^5$ s^{-1} is quite considerable.

4. Conclusion

The interaction of the molten AlMg alloy with a carbon-containing organic precursor under a layer of molten halides has been studied for the first time. The AlMgGr composites produced by the proposed method are compact and non-porous, with a characteristic metallic shine. It is shown by means of Raman spectroscopy and XPS that thin films of two- layer defective graphene are synthesized *in-situ* both at the Al-Mg matrix grain boundaries and inside the grains. The structure and phase composition of the AlMgGr composites in the cast and deformed ($\dot{\varepsilon}=1.3\times10^3$ s^{-1}) states were studied by light and electron microscopy. It has been established that graphene microalloying (up to 0.22%) of an AlMg alloy does not significantly affect its crystallization kinetics and deformation mechanism.

The mechanical properties of the AlMgGr composites under quasi-static and dynamic deformations have been studied. It has been established that the strengthening role of graphene increases with an increase in the dispersion of the matrix structure. If the formation of a fine-grained structure under dynamic compression causes a 10% increase in the conditional yield strength, then its further grinding to submicron sizes under the action of a plane shock wave already leads to a fourfold increase in the dynamic characteristics of the composite compared to the properties of an unreinforced alloy.

Acknowledgements. The results were obtained within the state assignments of Ministry of Science and Higher Education of the Russian Federation (IMP UB RAS, theme "Structure" № 122021000033-2, IHTE UB RAS, theme № 122020100210-9). The mechanical properties under shock-wave loading were investigated in IPCP RAS, theme №AAAA-A19-119071190040-5. The electron microscopic studies were performed at the Center of Collaborative Access Test Center of Nanotechnologies and Advanced Materials, Institute of Metal Physics, Ural Branch, Russian Academy of Sciences, Ekaterinburg. Shock-wave compression experiments were carried out using the equipment of Moscow Regional Explosive Research Center of Collective Use of the RAS. The Raman spectra for graphene were collected using the equipment of the Shared Access Center Composition of Compounds of Institute of High-Temperature Electrochemistry of the Ural Branch of the RAS, Ekaterinburg. XPS study was conducted by PhD V.I. Pryakhina using the equipment of the Ural Centre for Shared Use of Modern Nanotechnology at the Ural Federal University.

References

1. D.K. Das, P.C. Mishra, S. Singh, R.K. Thakur. Int. J. Mech. Mater. Eng. 9 (1), 12 (2014). Crossref
2. A.P. Khrustalev, A.A. Kozulin, I.A. Zhukov, M.G. Khmeleva, A.B. Vorozhtsov, D.G. Eskin, S. Chankitmunkong, V.V. Platov, S.V. Vasilev. Metals. 9 (10), 1030 (2019). Crossref
3. I.A. Zhukov, P.Y. Nikitin, M.V. Grigoriev, A.B. Vorozhtsov. Russ. Phys. J. 62 (5), 882 (2019). Crossref
4. P. Ashwath, M.A. Xavior. Procedia Engineering. 97, 1027 (2014). Crossref
5. Z. Hu, F. Chen, J. Xu, Q. Nian, D. Lin, C. Chen, X. Zhu, Y. Chen, M. Zhang. Journal of Alloys and Compounds. 746, 269 (2018). Crossref
6. L.F. Mondolfo. Aluminum Alloys: Structure and Properties. Butterworth & Co, London (1976). Crossref
7. S.R. Bakshi, D. Lahiri, A. Agarwal. International Materials Reviews. 55, 41 (2010). Crossref
8. Z. Hu, G. Tong, D. Lin, C. Chen, H. Guo, J. Xu, L. Zhou. Materials Science and Technology. 32 (9), 930 (2016). Crossref
9. L. Ci, Z. Ryu, N.Y. Jin-Phillipp, M. Rühle. Acta Materialia. 54, 5367 (2006). Crossref

10. R. Pérez-Bustamante, F. Pérez-Bustamante, I. Estrada-Guel, C. R. Santillán-Rodríguez, J. A. Matutes-Aquino, J. M. Herrera-Ramírez. Powder Technology. 212, 390 (2011). Crossref
11. A. G. Sheinerman. Physics of Metals and Metallography. 123, 57 (2022). Crossref
12. M. Bastwros, G.-Y. Kim, K. Zhang, S. Wang. Processing International Mechanical Engineering Congress and Exposition, ASME. San Diego, California, USA (2013) pp. 1–7.
13. L. A. Yolshina, R. V. Muradymov, I. V. Korsun, G. A. Yakovlev, S. V. Smirnov. J. Alloys and Compounds, 663, 449 (2016). Crossref
14. L. A. Yolshina, R. V. Muradymov, E. G. Vovkotrub, S. V. Smirnov. Diamond & Related Materials. 55, 1 (2015). Crossref
15. L. A. Yolshina, D. I. Vichuzhanin, E. O. Smirnova. AIP Conf. Proc. 1785, 040093 (2016). Crossref
16. L. A. Yolshina, E. G. Vovkotrub, A. A. Shatunova, V. I. Pryakhina. J. Raman Spectrosc. 51, 221 (2020). Crossref
17. I. G. Shirinkina, I. G. Brodova, D. Yu. Rasposienko, R. V. Muradymov, L. A. Yolshina, E. V. Shorokhov, S. V. Razorenov, G. V. Gorkushin. Physics of Metals and Metallography, 121 (12), 1193 (2020). Crossref
18. I. G. Brodova, A. N. Petrova, I. G. Shirinkina, D. Yu. Rasposienko, L. A. Yolshina, R. V. Muradymov, S. V. Razorenov, E. V. Shorokhov. Journal of Alloys and Compounds. 859, 158387 (2021). Crossref
19. A. N. Petrova, I. G. Brodova, O. A. Plekhov, O. B. Naimark, E. V. Shorokhov. Tech. Phys. 59, 989 (2014). Crossref
20. S. V. Razorenov. Matter Radi. at. Extremes. 3, 1 (2018). Crossref
21. M. Vanin, J. J. Mortensen, A. K. Kelkkanen, J. M. Garcia-Lastra, K. S. Thygesen, K. W. Jacobsen. Physical review B. 87, 081408 (2010). Crossref
22. R. Sharma, N. Chadha, P. Saini. Indian Journal of Pure & Applied Physics. 55, 625 (2017).
23. L. A. Yolshina, V. A. Yolshina, S. V. Pershina, V. I. Pryakhina. Diamond and Related Materials. 119, 108556 (2021). Crossref
24. Russian standart "GOST 4784-97", Wrought aluminium and aluminium alloys.
25. A. N. Petrova, I. G. Brodova, S. V. Razorenov, E. V. Shorokhov, T. K. Akopyan. Phys. Met. Metallogr. 120, 1221 (2019). Crossref
26. I. G. Brodova, A. N. Petrova, S. V. Razorenov, E. V. Shorokhov. Phys. Metals Metallogr. 116, 519 (2015). Crossref
27. I. G. Brodova, V. I. Zel'dovich, I. V. Khomskaya. Physics of Metals and Metallography. 121 (7), 631 (2020). Crossref
28. V. V. Malashenko. Physica B: Phys. Cond. Mat. 404 (21), 3890 (2009). Crossref